A THERMOMECHANICAL FATIGUE CRACK INITIATION MODEL FOR DIRECTIONALLY-SOLIDIFIED NI-BASE SUPERALLOYS

Ali P. Gordon[1], Mahesh Shenoy[1], and Richard W. Neu[12]

[1]The George W. Woodruff School of Mechanical Engineering, Atlanta, GA 30332-0405

[2]School of Materials Science and Engineering, Atlanta, GA 30332-0245

ABSTRACT

Nickel-base superalloys have been used extensively in power generation applications due to their high strength at temperatures up to 1093°C. When the material is subjected to complex mechanical loading superimposed with thermal loading, fatigue interacts with either creep and/or oxidation. Directionally-solidified (DS) materials are often used in place of polycrystalline (PC) materials since they derive their strength from the large directionally-oriented crystallographic grains. As a consequence, the propagation of microstructurally small cracks is controlled by certain microstructural features such as dendrite size, orientation and morphology, carbides in the interdendritic regions, oxide and gamma prime depleted layers. In this study a cumulative damage model capturing the key microstructural features influencing crack initiation is used to characterize a DS Ni-base superalloy with application to both longitudinal (L) and transverse (T) orientation. Both L and T specimens were used to carry out uniaxial *e*-controlled isothermal and thermomechanical fatigue (TMF) tests. The mechanistically-based model presented captures the combined effects of fatigue, creep, and oxidation on the formation of low cycle fatigue (LCF) cracks and the microstructurally small crack growth phase, both of which comprise the crack "initiation" stage. Key parameters that relate to the microstructure and affect the crack initiation life are included in the model.

1 INTRODUCTION

Directionally solidified (DS) Ni-base superalloys used in gas turbine components are subjected to extreme temperatures and environmental conditions. The life of these components is controlled by TMF and creep. With the elimination of grain boundaries (GBs) along the DS axis, corresponding to the radial axis of the blades, DS alloys have increased resistance to creep deformation and rupture. In addition, the lower elastic modulus in the [001] grain growth direction reduces the magnitude of cyclic inelastic strain under displacement control conditions associated with LCF. The combination of cyclic centrifugal forces experienced in blades at high temperatures in an aggressive environment coupled with the heterogeneity and inherent anisotropy of the microstructure can lead to one of several possible fatigue mechanisms. Consequently, any physically-based crack initiation model must capture the degradation mechanisms related to the microstructure and how they interact with the environment and cyclic inelastic behavior.

Reliable predictions can be made by understanding the different mechanisms for crack initiation that depend on mechanical loading, temperature, and microstructure features including crystallographic grain size and orientation; carbide volume fraction, size, morphology, and distribution; eutectic nodules; and secondary dendritic arm spacing. These *mechanistically*-based approaches rely on microstructural observations from a wide range of conditions. A separate model is conceived for each mechanism. Here, the total life includes crack nucleation and microcrack growth. For example, the total life, N_i, accounting for three possible dominant damage mechanisms, fatigue, creep-fatigue, and environment-fatigue damage, can be written [1]

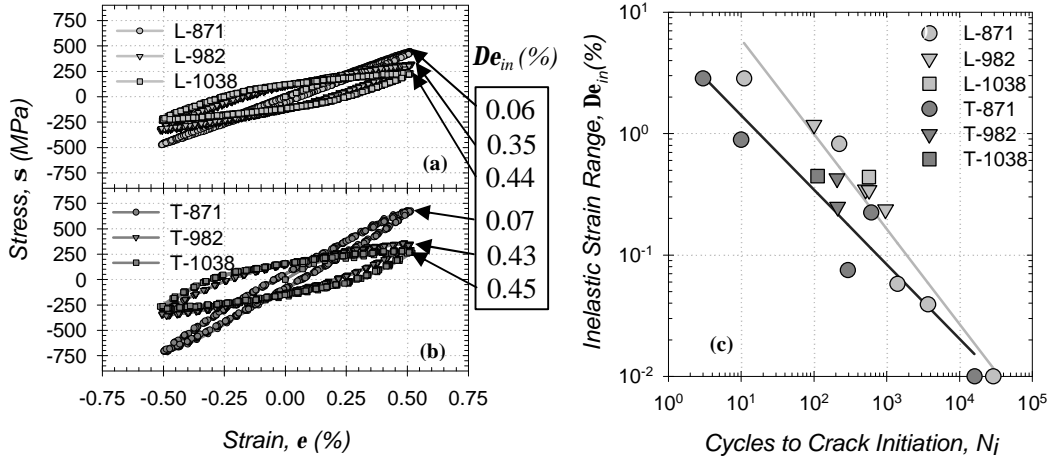$$\frac{1}{N_i} = \frac{1}{N_i^{fat}} + \frac{1}{N_i^{cr}} + \frac{1}{N_i^{env}} \qquad (1)$$

FIGURE 1: Initial responses of (a) L and (b) T specimens. (c) Inelastic strain crack initiation lives.

The *fatigue* term accounts for the generation and movement of dislocations when creep and environmental mechanisms are negligible. This term is often dependent on the heterogeneity of the microstructure including the size and distribution of inclusions, carbides, and eutectic nodules. In the simplest form, it is related to the mechanical strain range, $\boldsymbol{De}_m$, which relates to the local cyclic inelastic strains due to the heterogeneity of the microstructure, particularly near carbides and eutectics where cracks are observed to form. The *creep-fatigue* term is highly-dependent on the cyclic stress response, temperature, time, and the phasing between mechanical loading and temperature. The stress response needs to be captured by an accurate constitutive model that accounts for creep and crystallographic orientation of the grains. The *environment-fatigue* term relates the development and embrittlement of surface films (oxides and $\boldsymbol{g'}$ depleted zones) [2] with loading, temperature, and crystallographic orientation.

2 MATERIAL AND EXPERIMENTAL METHOD

The cast alloy DS GTD-111 was provided in the form of slabs with heat treatment typical of that used for components in gas turbine applications. In this DS Ni-base superalloy, the crystallographic grains are between 0.1 and 4 *mm* in diameter in the transverse direction. Major phases in the microstructure are the FCC Ni austenite matrix phase, termed $\boldsymbol{g}$, the $L1_2$-structured precipitate phase, known as $\boldsymbol{g'}$, hard carbides (MC and $M_{23}C_6$), and $\boldsymbol{g}$-$\boldsymbol{g'}$ eutectics [3]. Sizes of $\boldsymbol{g'}$ precipitate particles average 0.5 $\boldsymbol{mm}$ and account for between 45-65% of the total volume fraction.

Solid specimens with a gage section diameter of 6.35 *mm* were machined so that the grains were either longitudinally (L) or transversely (T) oriented with the loading direction. Several $\boldsymbol{e}$-controlled isothermal LCF tests were conducted at various temperatures using induction heating. Three cycle types were applied: continuous cycling with no hold time (CC), and cycling with holds in either tension (HT) or compression (HC). In TMF tests, specimens were subjected to superimposed temperature and mechanical strain cycling. Two baseline tests were conducted: linear in-phase (IP) and linear out-of-phase (OP). Tests were halted when the maximum load dropped below 80% of the initial stabilized response. This cycle is denoted as N_i.

3 OBSERVATIONS

Three primary crack initiation mechanisms were identified. At lower temperatures and under higher frequency cycling, the initiation of fatigue cracks was associated with a classical LCF mechanism associated with inelastic strain range, $\boldsymbol{De}_{in}$. As shown in Fig. 1, $\boldsymbol{De}_{in}$ controlled the
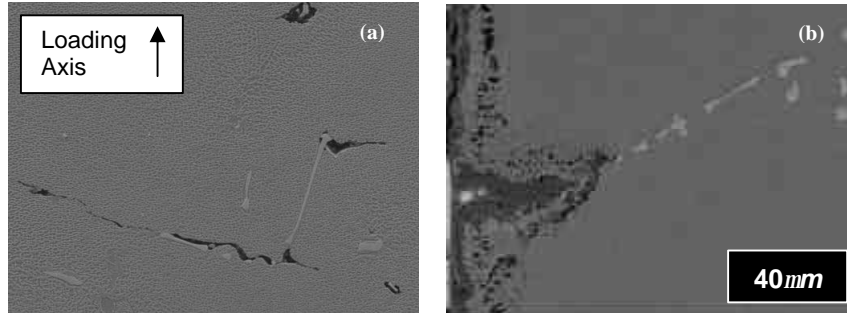
FIGURE 2: Influence of MC-type carbides on (a) subsurface and (b) surface crack initiation observed under LCF at 982ºC, 2min tension, $\mathbf{\mathit{De}}_{in}$=0.33%, after N_i=285.

fatigue-dominated crack initiation of both L and T-oriented DS GTD-111 specimens, with minimal temperature dependence within the range from 871 to 1038°C. However, at shorter lives, there is a crystallographic orientation dependence with T orientation having lower lives.

By incorporating 2 *min* dwells in tension or compression at 871°C and higher, the number of cycles leading to failure is reduced. Carbides and eutectics were found along the fracture surfaces of both types of samples. The particles act as stress raisers which facilitated localized inelastic deformation and loss of coherency at the interface. Their abundance at the fracture surface has importance since the overall volume fraction of carbides in the matrix is low. The majority of microcracks nucleating and growing at subsurfaces follow interdendritic channels or particles as illustrated in Fig. 2a. This is similar to the observations when primarily fatigue is operating. However, under creep-fatigue multiple creep-like voids appeared around several carbides and eutectics. The reduction in life is, therefore, related to fatigue coupled with a creep/diffusional degradation mechanism. Samples with the most pronounced internal microcracks and voids were those tested in the range of 871 and 982°C and with $\mathbf{\mathit{De}}_{in}$ between 0.33% and 0.66%. Lives with dwells are, as a result, shorter than those under CC by nearly 33% when $\mathbf{\mathit{De}}_{in}$ below 1.0%.

For tests operating at higher temperatures in an oxidizing environment (here, laboratory air) with oxide film forming, a coupling between environment and fatigue controls crack initiation. Furthermore, the heterogeneity of the microstructure plays an important role in that carbides near the surface more readily oxidize resulting in a more rapid degradation of their properties and hence are often preferred crack nucleation sites in the presence of an oxidizing environment (Fig. 2b). Under OP TMF cycling, an oxide spiking mechanism is promoted, shown in Fig. 3. This mechanism is described as the repeated tensile cracking of the surface film occurring at the maximum $\mathbf{\mathit{e}}_m$ and T_{min} levels when the film is most susceptible to brittle fracture. Oxidized carbides near the surface appear to accelerate this process. After a crack nucleates, it can grow through the same process of brittle fracture of films ahead of the crack tip. In Ni-base superalloys, the resulting film can be considerably complex. For example, as observed in Fig. 3, isothermal exposure at 982°C leads to thin Cr/Ti-rich oxide layer nearest the surface. Below that, Al-rich oxides form in a $\mathbf{\mathit{g}}$ matrix. Further from the surface, a softer $\mathbf{\mathit{g}}'$ depleted layer exists. Clearly, diffusion and oxidation kinetics must be incorporated into the model describing the environment-fatigue mechanism. Another related mechanism is oxide spallation which results from compressive stresses in the surface film usually due to mismatches in the coefficient of thermal expansion (CTE) between the surface film and substrate. This mechanism is particularly prevalent in IP TMF. At the minimum $\mathbf{\mathit{e}}_m$ and T_{min} level, unevenly distributed thermal strains accumulate across the oxide/metal interface since the CTE of oxidized material is nearly less than an order of magnitude of that for the base material. The combined thermal and compressive strains experienced in the cumulative oxidized
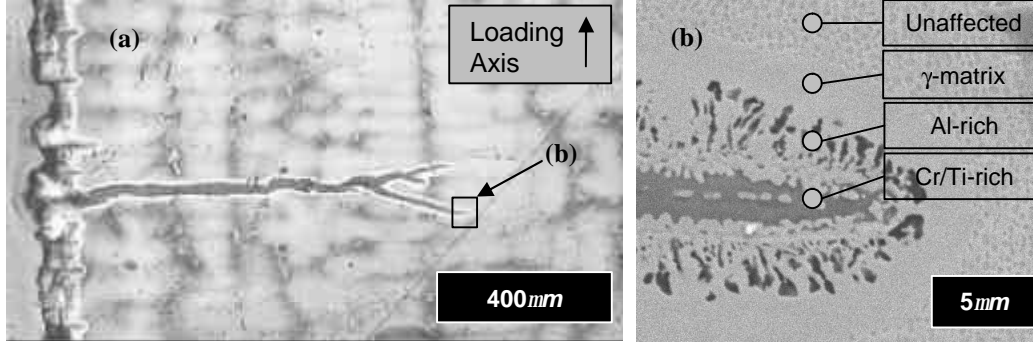
FIGURE 3: Oxide spiking in L DS GTD-111 after 69 hr at 982°C, De =0.5%, R_e=-1, and 2 min HC.

layer causes the surface film to wedge and detach from the substrate. Comparatively, the oxide spiking mechanism results in much deeper surface cracks than spallation, thus making OP cycling more detrimental to fatigue life than IP cycling.

The stress response of DS Ni-base materials under TMF is plotted with respect to the mechanical strain range, De_m, for several test cases in Fig. 4. Since both the elastic modulus and the yield strength are temperature dependent, the stress required to achieve the maximum and minimum strains are unequal. The consequence is positive mean stresses for OP cycling, and negative mean stresses for IP. Increasing De_m caused an increase in the portion of De_{in} for both L and T specimens, and, as expected, N_i decreased. For the range of conditions in Fig. 4c, the lives of CC isothermal specimens serve as an upper bound for TMF-tested samples. Hence, degradation under TMF includes contributions from environment-fatigue damage, along with perhaps a limited amount of creep-fatigue damage, both of which significantly hasten crack initiation compared to a condition when only fatigue damage mechanism operates.

4 LIFE PREDICTION

The crack initiation life can be predicted by simulating the cyclic response of the material under imposed isothermal and non-isothermal fatigue conditions. A viscoplasticity model [3] based on that developed by McDowell [4] was implemented in ABAQUS® as a user-defined material (UMAT). This model also includes anisotropic generalized Hooke's Law and crystallographic orientation effects. The viscoplastic flow rule describes the effects of dislocation motion to the macroscopic deformation of a grain. The shear strain rate on the ath slip system is given as

$$\dot{g}^{(a)} = \dot{g}_0 \Theta(T) \left\langle \frac{\left| t^{(a)} - c^{(a)} \right| - k^{(a)} \frac{m}{m_0}}{D_0} \right\rangle^n \exp\left\{ B_0 \left\langle \frac{\left| t^{(a)} - c^{(a)} \right| - k^{(a)} \frac{m}{m_0}}{D_0} \right\rangle^{n+1} \right\} Sgn\left(t^{(a)} - c^{(a)} \right) \quad (2)$$

where D_0 is the drag stress, $t^{(a)}$ is the resolved shear stress, and $c^{(a)}$ and $k^{(a)}$, are the back stress and threshold stress, respectively. Simulated hysteresis data (i.e., De_{in} and s) of a stabilized cycle is used to compute the accumulated fatigue, creep, and environmental damage.

Mathematic formulations were developed to relate each mechanism (*fat*, *cr*, and *env*) to temperature, grain orientation, hold times, etc. The fatigue damage mechanism is related by

$$N_i^{fat} = C_1 f_1 \left(\Delta e_{in} \right)^{C_2} \quad (3)$$

where C_1 and C_2 are constants and f_1 is a factor that accounts for material orientation (i.e., L or T) To characterize this relation, data is needed from low temperatures, high strain rates, and CC tests. Tests conducted at and below 871°C were used to correlate Eq. (3).
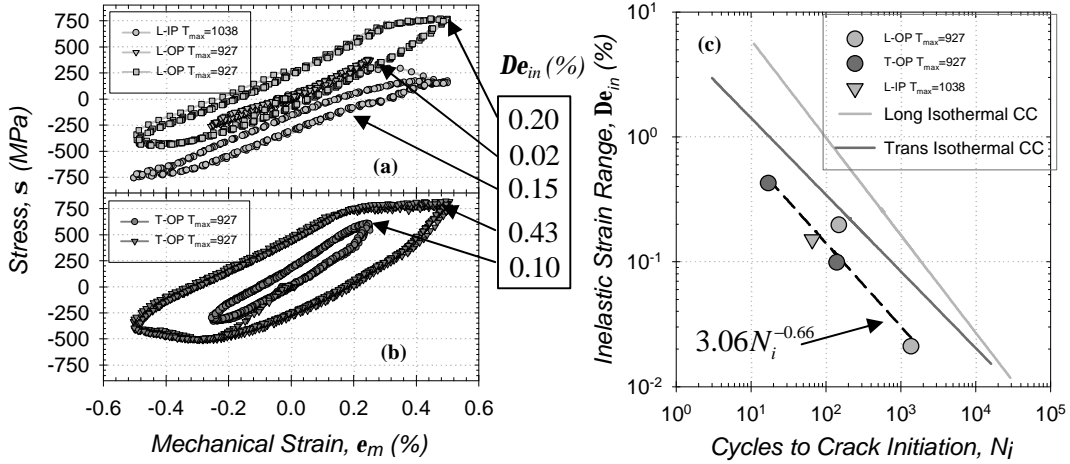
FIGURE 4: Initial stress-mechanical strain responses of TMF cycled (a) L and (b) T specimens. (c) Inelastic strain crack initiation lives for TMF and LCF (at 871°C) experiments.

The creep-fatigue interaction mechanism was found to correlate to

$$N_i^{cr} = C_3 \Theta_{cr}(T,t) \left(\frac{t_c + t_h}{t_c + 2t_h} \right)^{f_2} (\Delta e_{in})^{C_4} \tag{4}$$

where C_3, C_4, and f_2 are constants. The inelastic strain range, De_{in}, is used here since it captures orientation and time dependent deformation. The diffusion coefficient, Θ_{cr}, along with the cycle and dwell times, given by t_c an t_h, respectively, account for time and temperature-dependent degradation such as void nucleation and growth not captured in Eq. (3). The diffusion term is

$$\Theta_{cr}(T,t) = \frac{1}{t_c} \int_0^{t_c} \exp\left(-\frac{Q_{cr}}{RT(t)} \right) dt \tag{5}$$

Here Q_{cr} is the activation energy, $T(t)$ is the temperature history, and R is the gas constant. Specimens subjected to dwell times experience the most significant stress relaxation caused by viscoplastic deformation. The correlation of Eq. (4) involved HT and HC tests above 871°C.

The term relating environment-fatigue interaction to crack initiation is motivated by the oxide spiking mechanism. The interaction is related to cycle-dependent repeated fracture of the oxide film. This process is controlled by De_{el}, the oxidation growth kinetics, and the phasing between the mechanical and thermal loading captured through a phasing factor, Φ_{ox},

$$N_i^{ox} = C_5 \left[\Phi_{ox} \Theta_{ox}(t_c + t_h) \right]^{C_6} \Delta e_{el}^{C_7} \tag{6}$$

Here C_5, C_6, and C_7 are constants. The cycle time and diffusion factor, Θ_{ox}, similar to Eq. (5) with Q_{ox} capture the oxide film growth kinetics. The phasing factor is given by

$$\Phi_{ox} = \exp\left[-C_8 (\dot{e}_{th}/\dot{e}_m + 1)^2 \right] \tag{7}$$

This factor has a maximum value of unity for linear OP TMF, the condition most susceptible to the oxide spiking mechanism. Hysteresis data from isothermal tests above 871°C with dwells and TMF tests were used to determine the constants for Eqs. (6) and (7).

Some trends that the model predicts are shown in Fig. 5 for continuously-cycled L-oriented DS GTD-111 specimens. For both isothermal (Fig. 5a) and non-isothermal (Fig. 5b) cases, the crack initiation life is characterized by the constitutive response at high mechanical strain ranges since the fatigue term dominates. Under isothermal conditions, the change in slope of predicted life
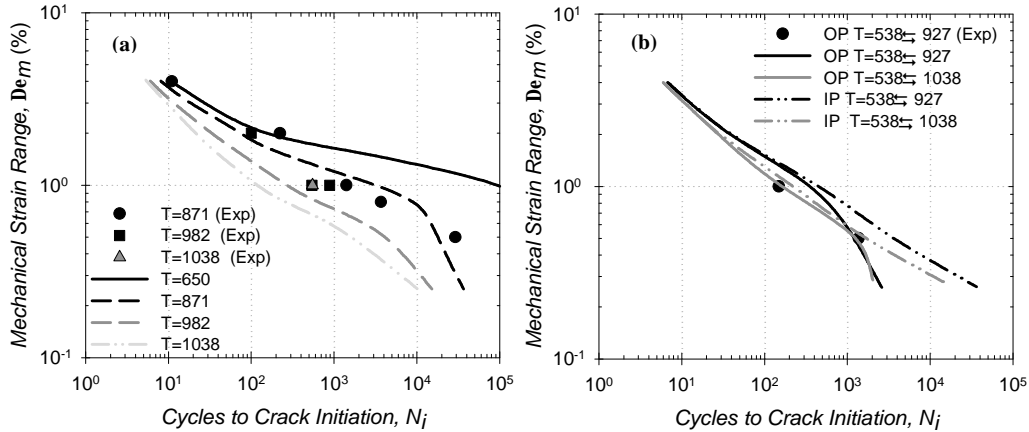
FIGURE 5: Predictions for (a) isothermal LCF and (b) TMF of L DS GTD-111 under CC.

below the mechanical strain range of 1.0% relates to a changeover from predominantly fatigue to coupled environment-fatigue mechanism. As the temperature is decreased below 871°C, there is insufficient thermodynamic energy to drive oxidation, and the role of environment is limited as a result. Under TMF conditions at lower mechanical strain ranges (Fig. 5b), the OP cycle is predicted to be more damaging than the IP cycle. This prediction is consistent with experiments since the oxide spiking, which is more detrimental to life than oxide spallation, is experienced during OP cycling. During IP cycling with De_m<1.0%, life is dominated by the fatigue mechanism. With the increase of DT from 389°C to 500°C, the constitutive model predicts De_{in} to increase. In identical sets of tests conducted when the mechanical strain range was the same for L and T-oriented DS GTD-111 specimens, the inelastic strain ranges for T specimens is greater as shown in Figs. 1 and 4. Consequently, the lives of L specimens typically outlast those of T on a basis of De_m. The crystallographic orientation dependence in the constitutive model captures this phenomenon, predicting the trends especially at higher mechanical strain ranges shown in Fig. 1.

5 CONCLUSIONS

Observations from experiments that isolated the microstructural mechanisms of fatigue, creep-fatigue, and environment-fatigue were used to formulate damage models for both L and T-oriented DS GTD-111. Under high frequency and isothermal conditions with De_{in}>1.0% and low temperatures, fatigue damage dominates. According to the prediction model, the contribution of the coupled creep-fatigue mechanism is increased with increasing temperature and/or cycle time; however, for each of the conditions considered, this mechanism remained a minor contributor to total damage. Tests with De_{in}<1.0% at high temperatures, including those with superimposed thermal cycling, are subject to environment-fatigue damage since the surface-related mechanisms are active at long exposure times.

References
1. Neu, R. W., and Sehitoglu, H., *Metallurgical Transactions A* **20**, 1989.
2. Sehitoglu, H., and Boismier, D. A., *Journal of Engineering Materials and Technology* **112**, 1990
3. Shenoy, M., Kang, M.-S., Neu, R. W., and McDowell, D. L., *in* "High-Temperature Fatigue, CAMP 2002," Paderborn, Germany, 2002.
4. McDowell, D. L., *International Journal of Plasticity* **8**, 1992.